AN ADAPTIVE DISCONTINUOUS GALERKIN MULTISCALE METHOD FOR ELLIPTIC PROBLEMS

DANIEL ELFVERSON[†§], EMMANUIL H. GEORGOULIS[‡XS] , AND AXEL MÅLQVIST[†¶]

Abstract. An adaptive discontinuous Galerkin multiscale method driven by an energy norm a posteriori error bound is proposed. The method is based on splitting the problem into a coarse and a fine scale. Localized fine scale constituent problems are solved on patches of the domain and are used to obtain a modified coarse scale equation. The coarse scale equation has considerably less degrees of freedom than the original problem. The a posteriori error bound is used within an adaptive algorithm to tune the critical parameters, i.e., the refinement level and the size of the different patches on which the fine scale constituent problems are solved. The fine scale computations are completely parallelizable, since no communication between different processors is required for solving the constituent fine scale problems. The convergence of the method, the performance of the adaptive strategy and the computational effort involved are investigated through a series of numerical experiments.

Key words. multiscale, discontinuous Galerkin, a posteriori error bound

AMS subject classifications. 65N30, 65N15

1. Introduction.

Problems involving features on several different scales, usually termed multiscale problems, can be found in many branches of the engineering sciences. Examples include the modelling of flow in a porous medium and of composite materials. Multiscale problems involving partial differential equations are often impossible to simulate with an acceptable accuracy using standard (single mesh) numerical methods. A different approach, usually coming under the general term of multiscale methods, consists of considering coarse and fine scale contributions to the solution, with the fine scale contributions approximated on localized patches. The fine scale contributions are then used to upscale the problem in order to obtain an approximation to the global multiscale solution.

1.1. Previous work.

Numerous multiscale methods have been developed during the last three decades, see e.g. [8, 7] for early works, or [16, 29, 15] and references therein for exposition and recent developments. An important development is the Multiscale finite element method (MsFEM) by Hou and Wu [21], which was further developed in [12], with the introduction of oversampling to reduce resonance effects. Another approach is the, so-called, Variational multiscale method (VMS) of Hughes and co-workers [22, 23]. The idea in VMS is to decompose the solution space into coarse and fine scale contributions. A modified coarse scale problem is then solved (using a finite element approach), so that the fine scale contribution is taken into account. To maintain the conformity of the resulting modified finite element space, homogeneous Dirichlet boundary conditions are imposed on each fine-problem patch boundary. The Adaptive variational multiscale method (AVMS) using the VMS framework, introduced by Larson and Målqvist [27], makes use of multiscale-type a posteriori error bound to adapt the coarse and fine scale mesh sizes as well as the fine-problem patch-sizes automatically. A priori error analysis can be found in [30].

[†]Information Technology, Uppsala University, SE-751 05, Uppsala, Sweden.
[‡]Department of Mathematics, University of Leicester, Leicester, UK.
[§]Supported by The Göran Gustafsson Foundation and The Swedish Research Council.
[¶]Supported by The Göran Gustafsson Foundation.

An interesting alternative to conforming finite element methods is the class of discontinuous Galerkin (DG) methods, whereby the approximation spaces are elementwise discontinuous; the continuity of the underlying exact solutions is imposed weakly. DG methods appeared in the 1970s and in the early 1980s [32, 28, 9, 5, 24] and have recently received renewed interest; we refer to the volumes [13, 14, 20, 33] and the references therein for a literature review. DG methods admit good conservation properties of the state variable and, due to the lack of inter-element continuity requirements are ideally suited for application to complex and/or irregular meshes. Also, there has been work to better cope with the case of high contrast diffusion; see e.g. [19] where a DG method based on weighted average is proposed and analysed. Discontinuous Galerkin methods for solving multiscale problems have been discussed using the framework of the MsFEM [1] and of the Heterogeneous multiscale method (HMM) [2]; see also [37, 36, 35, 34]. An a priori error analysis for the class of discontinuous Galerkin multiscale method studied in this paper can be found in [17].

1.2. New contributions. In this work, we propose an *adaptive discontinuous Galerkin multiscale method* (ADG-MS) using the framework of VMS. The underling DG method is based on weighted averages across the element interfaces. The adaptivity is driven by energy norm a posteriori error bounds. The multiscale method is based on solving localized problems on patches, which are then upscaled to solve a coarse scale equation. The lack of inter-element continuity requirements of the approximate solution, allows for very general meshes which is very common in multiscale applications, i.e. meshes that contains several types of elements and/or hanging nodes. The split between the coarse and fine sale is realized using the elemetwise L^2-projection onto the coarse mesh. This is more natural in a multiscale setting than e.g. using the nodal interpolant as in [27]. It is also much easier and efficient to construct an L^2 orthogonal split using DG rather then CG. The ADG-MS inherits a local conservation property from DG on the coarse scale, which is crucial in many applications such as porous media flow. The fine scale problems can be solved independently with localized right hand sides, and it is known that the solutions decay exponentially [17], which allows for small patches. In this case the ADG-MS converge to the reference solution and thereby takes full advantage of cancellation between patches, this is not the case for AVMS [27] since hanging nodes is not allowed. In the a posteriori error bound, the error is bounded in terms of the size of the different fine-scale patches and on both the fine-scale and the coarse-scale mesh sizes. An adaptive algorithm to tune all these parameters automatically is proposed. The numerical experiments show good performance of the algorithm for a number of benchmark problems.

1.3. Outline. The rest of this work is structured as follows. Section 2 is devoted to setting up the model problem, the basic DG discretization and some notation. A general framework for multiscale problems along with the discontinuous Galerkin multiscale method is derived in Section 3, and the a posteriori error bound is derived in Section 4. The implementation of the method and the adaptive algorithm are discussed in Section 5. In Section 6, a number of numerical experiments are presented, and finally some conclusions are drawn in Section 7.

2. Preliminaries. In this section we define some notations and the underling DG method is presented.

2.1. Notation. Let $\omega \subseteq \mathbb{R}^d$, $d = 2, 3$ be an open polygonal domain. Denote the $L^2(\omega)$-inner product by $(\cdot,\cdot)_{L^2(\omega)}$, and the corresponding norm by $\|\cdot\|_{L^2(\omega)}$. Also, let $H^1(\omega)$ be the Sobolev space with norm $\|\cdot\|_{H^1(\omega)} := (\|\cdot\|^2_{L^2(\omega)} + \|\nabla\cdot\|^2_{L^2(\omega)})^{1/2}$ and

$H^s(\omega)$ the standard Hilbertian Sobolev space of index $s \in \mathbb{R}$. We shall also make use of the space $L^\infty(\omega)$ consisting of almost everywhere bounded functions, with norm $\|\cdot\|_{L^\infty(\omega)} := \text{ess sup}_\omega|\cdot|$; see, e.g., [3] for details. Finally, the d-dimensional Lebesgue measure will be denoted by $\mu_d(\cdot)$.

2.2. The Model problem. Let $\Omega \subset \mathbb{R}^d$ be an open polygonal domain with Lipschitz boundary $\partial\Omega$, $d = 2, 3$, and consider the elliptic boundary value problem find $u \in \{v \in H^1(\Omega) : v|_{\partial\Omega} = 0\}$ fulfilling

$$-\nabla \cdot A\nabla u = f \qquad u \in \Omega, \tag{2.1}$$

$$u = 0 \qquad u \in \partial\Omega, \tag{2.2}$$

with $f \in L^2(\Omega)$ and $A \in L^\infty(\Omega, \mathbb{R}^{d,d}_{\text{sym}})$ such that A has uniform spectral bounds, bounded below by $\alpha > 0 \in \mathbb{R}$ almost everywhere.

2.3. Discretization and subdivision. The domain Ω is subdivided into a partition $\mathcal{K} = \{K\}$ of shape-regular and closed elements K with boundaries ∂K, i.e. $\bar{\Omega} = \cup_{K\in\mathcal{K}}\bar{K}$. On the partition $\mathcal{K}$, let $h : \cup_{K\in\mathcal{K}}K \to \mathbb{R}$ be a mesh-function defined element-wise by $h|_K := \text{diam}(K)$, $K \in \mathcal{K}$. The partition is allowed to be irregular (i.e. hanging nodes are allowed) and it is locally quasi uniform in the sense that the ratio of the mesh function h for neighboring elements is uniformly bounded from above and below. Let Γ^B be the set of all boundary edges and Γ^I be the set of all interior edges (or faces when $d = 3$) such that $\Gamma = \Gamma^B \cap \Gamma^I$ is the set of all edges in the partition $\mathcal{K}$. Associated with the diffusion tensor, we consider the element-wise constant functions $A^0, A_0 : \cup_{K\in\mathcal{K}}K \to \mathbb{R}$ defined by the biggest and smallest eigenvalue of A, respectively, on each element K. For $K_i, K_j \in \mathcal{K}$, with $\mu_{d-1}(\partial K_i \cap \partial K_j) > 0$, let K_i, K_j be denoted by K^+ and K^-, where K^+ is the element with the higher index. On interior element interfaces $e \in \Gamma^I$ we shall make use of the shorthand notation $v^+ := v|_{K^+}$, $v^- := v|_{K^-}$; on boundary edges we set $v^+ := v|_K$. We also define the weighted mean value by

$$\{v\}_w := w_{K^+(e)}v^+ + w_{K^+(e)}v^-, \tag{2.3}$$

where

$$w_{K^+(e)} := \frac{A^0|_{K^-}}{A^0|_{K^+} + A^0|_{K^-}}, \qquad w_{K^-(e)} := \frac{A^0|_{K^+}}{A^0|_{K^+} + A^0|_{K^-}}, \tag{2.4}$$

for each $e \in \Gamma^I$ and

$$w_{K^+(e)} = 1, \qquad w_{K^+(e)} = 0, \tag{2.5}$$

for $e \in \Gamma^B$. Further, the jump across element interfaces is defined by

$$[v] := v^+ - v^- \text{ for } e \in \Gamma^I, \qquad \text{and} \qquad [v] := v^+ \text{ for } e \in \Gamma^B, \tag{2.6}$$

and the harmonic mean value γ_e by

$$\gamma_e := \frac{2A^0|_{K^+} \cdot A^0|_{K^-}}{A^0|_{K^+} + A^0|_{K^-}}. \tag{2.7}$$

Also, n will denote the outward unit normal to ∂K^+ when $\mu_{d-1}(\partial K^+ \cap \partial K^-) > 0$. When $\mu_{d-1}(\partial K \cap \partial\Omega) > 0$, n will be the outward unit normal to $\partial\Omega$.

2.4. The Discontinuous Galerkin method. For a nonnegative integer r, we denote by $\mathcal{P}_r(\hat{K})$, the set of all polynomials on $\hat{K}$ of total degree at most r, if $\hat{K}$ is the reference d-simplex or, of degree at most r in each variable, if $\hat{K}$ the reference d-hypercube.

Consider the space $\mathcal{V} := \mathcal{V}_h + H^{1+\epsilon}(\Omega)$ with $\epsilon > 0$ but arbitrary small, and let the discontinuous finite element space be given by

$$\mathcal{V}_h := \{v \in L^2(\Omega) : v \circ F_K|_K \in \mathcal{P}_r(\hat{K}),\, \hat{K} \in \mathcal{K}\}, \tag{2.8}$$

where $F_K : \hat{K} \to K$ is the respective elemental map for $K \in \mathcal{K}$.

The discontinuous Galerkin method then reads: find $u_h \in \mathcal{V}_h$ such that

$$a(u_h, v) = \ell(v), \quad \forall v \in \mathcal{V}_h, \tag{2.9}$$

where the bilinear form $a(\cdot,\cdot) : \mathcal{V} \times \mathcal{V} \to \mathbb{R}$ and the linear form $\ell(\cdot) : \mathcal{V} \to \mathbb{R}$ are given by

$$\begin{aligned} a(v,z) :=& \sum_{K\in\mathcal{K}} (A\nabla v, \nabla z)_{L^2(K)} - \sum_{e\in\Gamma} \Big((n \cdot \{A\Pi\nabla v\}_w, [z])_{L^2(e)} \\ &+ (n \cdot \{A\Pi\nabla z\}_w, [v])_{L^2(e)} - \frac{\sigma_e\gamma_e}{h_e}([v],[z])_{L^2(e)} \Big), \end{aligned} \tag{2.10}$$

$$\ell(v) :=(f,v)_{L^2(\Omega)}, \tag{2.11}$$

respectively. Here $\Pi : (L^2(\Omega))^d \to (\mathcal{V}_h)^d$ denotes the orthogonal L^2-projection operator onto $(\mathcal{V}_h)^d$, $h_e := \mathrm{diam}(e)$, and $\sigma_e \in \mathbb{R}$ is a positive constant. The bilinear form (2.11) is coercive with respect to the natural energy norm,

$$|||v||| = \left(\sum_{K\in\mathcal{K}} \|A^{1/2}\nabla v\|^2_{L^2(K)} + \sum_{e\in\Gamma} \frac{\sigma_e\gamma_e}{h_e} \|[v]\|^2_{L^2(e)} \right)^{1/2} \tag{2.12}$$

if σ_e is chosen to be large enough. We refer, e.g., to [14, 6] and references therein for details on the analysis of DG methods for elliptic problems. Discontinuous Galerkin methods with weighted averages were introduced in [10, 19].

REMARK 2.1. *For all $v \in \mathcal{V}_h$, we have $\Pi\nabla v = \nabla v$, therefore the bilinear form* (2.10) *with $v, z \in \mathcal{V}_h$ is reduced to the more familiar form*

$$\begin{aligned} a(v,z) =& \sum_{K\in\mathcal{K}} (A\nabla v, \nabla z)_{L^2(K)} - \sum_{e\in\Gamma} \Big((n \cdot \{A\nabla v\}_w, [z])_{L^2(e)} \\ &+ (n \cdot \{A\nabla z\}_w, [v])_{L^2(e)} - \frac{\sigma_e\gamma_e}{h_e}([v],[z])_{L^2(e)} \Big). \end{aligned} \tag{2.13}$$

3. The Multiscale method. In the VMS framework, the finite element solution space $\mathcal{V}_h$ is decoupled into coarse and fine scale contributions, viz., $\mathcal{V}_h = \mathcal{V}_H \oplus \mathcal{V}_f$, with $\mathcal{V}_H \subset \mathcal{V}_h$. To this end, let $\Pi_H : L^2(\Omega) \to \mathcal{V}_H$ be the (ortogonal) L^2-projection onto the coarse mesh. The split between the coarse and fine scales is then determined by, $\mathcal{V}_H := \Pi_H\mathcal{V}_h$ and $\mathcal{V}_f := (I - \Pi_H)\mathcal{V}_h = \{v \in \mathcal{V}_h : \Pi_H v = 0\}$ where I is the identity operator.

The multiscale map $\mathcal{T} : \mathcal{V}_H \to \mathcal{V}_f$ from the coarse to the fine scale is defined as

$$a(\mathcal{T}v_H, v_f) = -a(v_H, v_f) \quad \forall v_H \in \mathcal{V}_H \text{ and } \forall v_f \in \mathcal{V}_f. \tag{3.1}$$

The next step is to decompose u_h and v in (2.9) into coarse and fine scale components. In particular, we have

$$u_h = u_H + \mathcal{T}u_H + u_f, \tag{3.2}$$

and $v = v_H + v_f$, with $u_H, v_H \in \mathcal{V}_H$ and $\mathcal{T}u_H, v_f \in \mathcal{V}_f$, for some $u_f \in \mathcal{V}_f$. Equation (2.9) is equivalent to the problem: find $u_H \in \mathcal{V}_H$ and $v_f \in \mathcal{V}_f$ such that

$$a(u_H + \mathcal{T}u_H + u_f, v_H + v_f) = \ell(v_H + v_f), \quad \forall v_H \in \mathcal{V}_H \text{ and } \forall v_f \in \mathcal{V}_f. \tag{3.3}$$

The fine scale component u_f can be computed by letting $v_H = 0$ in (3.3) and using the multiscale map (3.1). We obtain the fine scale problem driven by the right hand side data f: find $u_f \in \mathcal{V}_f$ such that

$$a(u_f, v_f) = \ell(v_f), \quad \forall v_f \in \mathcal{V}_f. \tag{3.4}$$

The coarse scale solution is obtained by letting $v_f = 0$ in (3.3): find $u_H \in \mathcal{V}_H$ such that

$$a(u_H + \mathcal{T}u_H, v_H) = \ell(v_H) - a(u_f, v_H), \quad \forall v_H \in \mathcal{V}_H. \tag{3.5}$$

In (3.5), $\mathcal{T}v_H$ and u_f are unknown and obtained by solving (3.1) and (3.4). Note that the linear system (3.5) has $\dim(\mathcal{V}_H)$ unknowns.

3.1. Localization and Discretization. The bilinear form is characterized by more local behavior in $\mathcal{V}_f$ than in $\mathcal{V}_h$ [30, 17]. This motivates us to solve the fine scale equations on (localized) overlapping patches, instead of the whole domain Ω. The patches are chosen large enough to ensure sufficiently accurate computations of $\mathcal{T}v_H$ and u_f. The computations of the fine scale components of the solution can be done in parallel with localized right hand sides. To define the coarse space $\mathcal{V}_H$, we begin by fixing a coarse mesh $\mathcal{K}_H$. Then, $\mathcal{V}_H$ is defined as,

$$\mathcal{V}_H := \{v \in L^2(\Omega) : v \circ F_K|_K \in \mathcal{P}_r(\hat{K}),\ \hat{K} \in \mathcal{K}_H\}. \tag{3.6}$$

DEFINITION 3.1. *For all $K \in \mathcal{K}_H$, define element patches of size L patch as*

$$\begin{aligned} \omega_K^1 &= int(K) \\ \omega_K^L &= int(\cup\{K' \in \mathcal{K}_H \mid K' \cap \bar{\omega}_K^L\}), \quad L = 2, 3, \ldots. \end{aligned} \tag{3.7}$$

The patch ω_K^L will be refered to as a L-layer patch. This is illustrated in Figure 3.1.

On each L-layer patch, we let $\mathcal{K}(\omega_K^L)$ be a restiction of $\mathcal{K}$ to ω_K^L, such that $\cup_{K \in \mathcal{K}(\omega_K^L)} = \bar{\omega}_K^L$. Also let $\Gamma^I(\omega_K^L)$ and $\Gamma^B(\omega_K^L)$ be the interior respectively boundary edges on $\mathcal{K}(\omega_K^L)$. Moreover, we assume that $\mathcal{K}_H|_{\omega_K^L}$ and $\mathcal{K}(\omega_K^L)$ are nested, that is, every coarse element $K_H \in \mathcal{K}_H|_{\omega_K^L}$ coincides with a union of fine elements $K \in \mathcal{K}(\omega_K^L)$. Also, the fine test spaces $\mathcal{V}_f(\omega_K^L)$, are defined by

$$\mathcal{V}_f(\omega_K^L) := \{v \in \mathcal{V}_f : v|_{\Omega \setminus \omega_K^L} = 0\}. \tag{3.8}$$

Finally, let the indicator function be $\chi_K = 1$ on element K and 0 otherwise and $\mathcal{M}_K$ be the index set of all basis functions $\phi_j \in \mathcal{V}_H$ that have support on K i.e., $\chi_K = \sum_{j \in \mathcal{M}_K} \phi_j$.

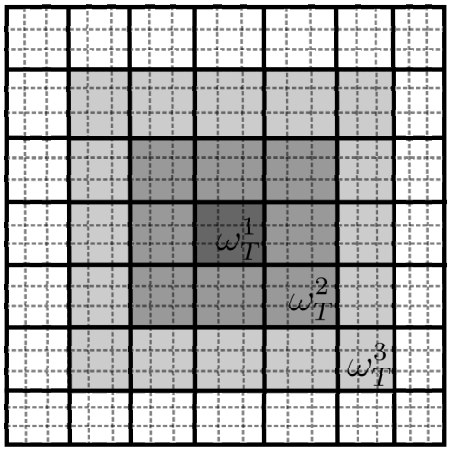

FIGURE 3.1. *Example of a one ω_K^1, two ω_K^2, and three ω_K^3 layer patches around element T in a quadrilateral mesh.*

3.2. The Discontinuous Galerkin Multiscale method. For each $K \in \mathcal{K}_H$ the following local problems need to be solved: find $\tilde{\mathcal{T}}\phi_j \in \mathcal{V}_f(\omega_K^L)$, $\forall j \in \mathcal{M}_K$ and $U_{f,K} \in \mathcal{V}_f(\omega_K^L)$ such that

$$a(\tilde{\mathcal{T}}\phi_j, v_f) = -a(\phi_j, v_f), \quad \forall v_f \in \mathcal{V}_f(\omega_K^L), \tag{3.9}$$

$$a(U_{f,K}, v_f) = \ell(\chi_K v_f), \quad \forall v_f \in \mathcal{V}_f(\omega_K^L). \tag{3.10}$$

The modified coarse scale problem is formulated as: find $U_H \in \mathcal{V}_H$ such that

$$a(U_H + \tilde{\mathcal{T}}U_H, v_H) = \ell(v_H) - a(U_f, v_H), \quad \forall v_H \in \mathcal{V}_H, \tag{3.11}$$

where $U_f := \sum_{K\in\mathcal{K}_H} U_{f,K}$. The approximate solution to the multiscale problem is given by

$$U = U_H + \tilde{\mathcal{T}}U_H + U_f. \tag{3.12}$$

The above procedure will be referred to as the *discontinuous Galerkin multiscale method*.

We note that the approximation U is *not* equal to u_h in general, since the domains of the fine scale problems are truncated. However, as discussed above it is expected that U is a good approximation to u_h, due to the decaying nature of the fine scale solutions away from the respective patch. For the approximation U to converge to the exact solution u in (2.1) in the limit, both the support of the local problems need to be increase to the whole domain and the fine scale mesh-parameter need to decrease, $h \to 0$. The multiscale method proposed here differs from the one proposed in [17], in that a right hand side correction is present. Using the formulation without the presense a right hand side correction, the multiscale solution converge to a some H-perturbation of the exact solution u.

REMARK 3.2. *Note that for a non-uniform mesh $\mathcal{K}$ (and/or $\mathcal{K}_H$), the convergence results presented in [17] still hold if the corrected basis function are computed on patches of a common reference mesh $\mathcal{K}$. On the other hand if the adaptive algorithm is used such that the overlap between different corrected basis functions are computed on different meshes (e.g. [27]), less cancellation of the error will occue and convergence can no longer be guarantied by the argument in [17].*

3.3. Local conservation property. The DG methods are known to have good local conservation properties in that the normal fluxes are conservative. The ADG-MS inherits this property on the coarse scale. To see this, we introduce the normal fluxes on element $K_H \in \mathcal{K}_H$ as

$$\hat{\sigma}(U) := (\{n \cdot A\nabla U\}_w - \sigma_e \gamma_e h_e^{-1}[U])[\chi_{K_H}], \quad e \in \partial K_H, \tag{3.13}$$

where $U = U_H + \tilde{\mathcal{T}} U_H + U_f$, $\chi_{K_H} = 1$ on element K_H and $\chi_{K_H} = 0$ otherwice ($[\chi_{K_H}]$ is either 1 or -1), and each interface e is a face of a fine scale element $K \in \mathcal{K}$, i.e., the number of edges can exceed the number of faces for each element K_H. By setting $w \in \mathcal{V}_H$ to be $w = \chi_{K_H}$ in (2.10), (2.11), and by using the discrete normal fluxes defined in (3.13), we arrive to the discrete element-wise conservation law

$$(f, 1)_{L^2(K_H)} + (\hat{\sigma}(U), 1)_{L^2(\partial K_H)} = 0, \tag{3.14}$$

for all $K_H \in \mathcal{K}_H$.

4. A Posteriori Error Bound in Energy Norm. Let the constant $0 \leq C < \infty$ be any generic constant neither depending on H, h, L, nor A; let $a \lesssim b$ abbreviates the inequality $a \leq Cb$. The following approximation results will be used frequently throughout this section. Let π be the orthogonal L^2-projection operator onto element-wise constant functions. Then π satisfies the following approximation properties: for an element K, we have

$$||v - \pi v||_{L^2(K)} \lesssim \frac{h_K}{\sqrt{A_0}} ||A^{1/2}\nabla v||_{L^2(K)}, \quad \forall v \in H^1(K), \tag{4.1}$$

$$||v - \pi v||_{L^2(\partial K)} \lesssim \sqrt{\frac{h_K}{A_0}} ||A^{1/2}\nabla v||_{L^2(K)} \quad \forall v \in H^1(K). \tag{4.2}$$

LEMMA 4.1. *Let $\mathcal{I}_h^c : \mathcal{V}_h \to \mathcal{V}_h \cap H^1(\Omega)$ be a averging interpolation operator defined pointwise as*

$$\mathcal{I}_h^c v_h(\tilde{x}) = \frac{1}{|\mathcal{K}_{\tilde{x}}|} \sum_{K \in \mathcal{K}_{\tilde{x}}} v_h(\tilde{x})|_K, \tag{4.3}$$

where $\mathcal{K}_{\tilde{x}}$ is the set of elements in $\mathcal{K}$ for which $\tilde{x}$ belong, with the cardinal $|\mathcal{K}_{\tilde{x}}|$. Then,

$$||v_h - \mathcal{I}_h^c v_h||^2_{L^2(K)} \lesssim ||\sqrt{h_e}[v_h]||^2_{L^2(\partial K)}, \tag{4.4}$$

$$||A^{1/2}\nabla(v_h - \mathcal{I}_h^c v_h)||^2_{L^2(K)} \lesssim A^0 || \frac{1}{\sqrt{h_e}}[v_h]||^2_{L^2(\partial K)}. \tag{4.5}$$

holds for all $v_h \in \mathcal{V}_h$ and $K \in \mathcal{K}$.

The proof, omitted here, follows closely that of [25]. Lemma 4.1 can also be extended to irregular meshes. There a hierarchical refinement of the mesh is performed to eliminate the hanging nodes; we refer to [26] for details. For irregular meshes the constant in the bounds of Lemma 4.1 also depends on the number of hanging nodes on each face.

REMARK 4.2. *The result in Lemma 4.1 can be sharpened if the diffusion tensor is isotropic and a locally quasi-monotone [31] distribution is assumed to hold. Then $A^0|_K$ can be replaced by the harmonic mean value γ_e on face e; see [11].*

First we derive a posteriori error bound for the underling (one scale) DG method.

THEOREM 4.3. *Let u, u_h be given by* (2.1)-(2.2) *and* (2.9)*, respectively. Let also $\mathcal{I}_h^c u_h \in \mathcal{V}_h \cap H^1(\Omega)$ be given by* (4.3)*. Moreover, let $\mathcal{E} := \mathcal{E}_c + \mathcal{E}_d$ where $\mathcal{E}_c := u - \mathcal{I}_h^c u_h$ and $\mathcal{E}_d := \mathcal{I}_h^c u_h - u_h$. Then*

$$|||\mathcal{E}||| \lesssim (\sum_{K\in\mathcal{K}} \varrho_K^2)^{1/2} + (\sum_{K\in\mathcal{K}} \zeta_K^2)^{1/2}, \tag{4.6}$$

where

$$\begin{aligned}\varrho_K &= \frac{h_K}{\sqrt{A_0}}||(1-\Pi)(f+\nabla\cdot A\nabla u_h)||_{L^2(K)}, \qquad (4.7)\\ &\quad +\sqrt{\frac{h_K}{A_0}}\Big(||(1-w_{K(e)})n\cdot[A\nabla u_h]||_{L^2(\partial K\setminus\Gamma^B)} + ||\frac{\sigma_e\gamma_e}{h_e}[u_h]||_{L^2(\partial K)}\Big),\\ \zeta_K^2 &= ||A^{1/2}\nabla(u_h - \mathcal{I}_h^c u_h)||_{L^2(K)}^2 + ||\sqrt{\frac{\sigma_e\gamma_e}{h_e}}[u_h]||_{L^2(\partial K)}^2. \qquad (4.8)\end{aligned}$$

REMARK 4.4. *Using $\mathcal{I}_h^c u_h$ as the conforming part of u_h, we arrive to an a posteriori bound whereby $\mathcal{I}_h^c u_h$ can either be evaluated directly, or bounded using Lemma 4.1. Another possible choice is a weighted averging interpolation operator with the weights depending on the diffusion tensor [4].*

REMARK 4.5. *Concerning the lower efficiency bounds, the term* (4.7) *is robust with respect to the diffusion tensor; see [18]. But to prove that* (4.8) *is robust with respect to the diffusion tensor, to the authors' knowledge, the diffusion tensor has to be isotropic and satisfy a locally quasi-monotone property [31, 11].*

Proof. Note that

$$|||\mathcal{E}||| \le |||\mathcal{E}_c||| + |||\mathcal{E}_d|||, \tag{4.9}$$

where the first part can be bounded by

$$|||\mathcal{E}_c|||^2 \lesssim a(\mathcal{E}_c,\mathcal{E}_c) = a(\mathcal{E},\mathcal{E}_c) - a(\mathcal{E}_d,\mathcal{E}_c) \lesssim a(\mathcal{E},\mathcal{E}_c) + |||\mathcal{E}_d||||||\mathcal{E}_c|||. \tag{4.10}$$

Let π_h be the L^2-orthogonal projection onto the element-wise constant functions and define $\eta := \mathcal{E}_c - \pi_h\mathcal{E}_c$. We then have

$$a(\mathcal{E},\mathcal{E}_c) = a(u,\mathcal{E}_c) - a(u_h,\mathcal{E}_c) = \ell(\mathcal{E}_c) - a(u_h,\mathcal{E}_c) = \ell(\eta) - a(u_h,\eta), \tag{4.11}$$

which implies

$$|||\mathcal{E}_c|||^2 = a(\mathcal{E}_c,\mathcal{E}_c) = \big(\ell(\eta) - a(u_h,\eta)\big) - a(\mathcal{E}_d,\mathcal{E}_c). \tag{4.12}$$

Upon integration by parts and using the identity $[vw] = \{v\}_w[w] + \{w\}_{\bar w}[v]$ where $\bar w$ is the skew-weighted average given by

$$\{v\}_{\bar w} := w_{K^-(e)}v^+ + w_{K^+(e)}v^-, \tag{4.13}$$

the first term on the right-hand side of (4.12) yields

$$\begin{aligned}&\ell(\eta) - a(u_h,\eta)\\ &= \sum_{K\in\mathcal{K}}(f+\nabla\cdot A\nabla u_h,\eta)_{L^2(K)} + \sum_{e\in\Gamma}\Big(-(n\cdot[A\nabla u_h],\{\eta\}_{\bar w})_{L^2(e\setminus\Gamma^B)} \qquad (4.14)\\ &\quad +(n\cdot\{A\Pi\nabla\eta\}_w,[u_h])_{L^2(e)} - \sigma\gamma_e h_e^{-1}([u_h],[\eta])_{L^2(e)}\Big).\end{aligned}$$

The first term on the right-hand side of (4.14) can be bounded as follows,

$$\sum_{K\in\mathcal{K}}(f+\nabla\cdot A\nabla u_h,\eta)_{L^2(K)} \lesssim \sum_{K\in\mathcal{K}}\frac{h_K}{\sqrt{A_0}}||(1-\Pi)(f+\nabla\cdot A\nabla u_h)||_{L^2(K)}||A^{1/2}\nabla\mathcal{E}_c||_{L^2(K)},$$

using (4.1). The second term on the right-hand side of (4.14) gives

$$\begin{aligned}&\sum_{e\in\Gamma\setminus\Gamma^B}(n\cdot[A\nabla u_h],\{\eta\}_{\bar{w}})_{L^2(e)} \qquad (4.15)\\ &\lesssim \sum_{K\in\mathcal{K}}\sqrt{\frac{h_K}{A_0}}||(1-w_{K(e)})n\cdot[A\nabla u_h]||_{L^2(\partial K\setminus\Gamma^B)}||A^{1/2}\nabla\mathcal{E}_c||_{L^2(K)},\end{aligned}$$

using (4.2). For the third term on the right-hand side of (4.14), noting that $\nabla\eta=\nabla\mathcal{E}_c$, we deduces

$$\sum_{e\in\Gamma}(n\cdot\{A\Pi\nabla\mathcal{E}_c\}_w,[\mathcal{E}_d])_{L^2(e)} \lesssim \sum_{K\in\mathcal{K}}\frac{1}{\sqrt{h_K A_0}}||\gamma_e[\mathcal{E}_d]||_{L^2(\partial K)}||A^{1/2}\nabla\mathcal{E}_c||_{L^2(K)},$$

using an inverse estimate and the L^2-stability of Π. For the last term on the right-hand side of (4.14), we have

$$\sum_{e\in\Gamma}\frac{\sigma_e\gamma_e}{h_e}([u_h],[\eta])_{L^2(e)} \lesssim \sum_{K\in\mathcal{K}}\sqrt{\frac{h_K}{A_0}}||\frac{\sigma_e\gamma_e}{h_e}[u_h]||_{L^2(\partial K\setminus\Gamma^B)}||A^{1/2}\nabla\mathcal{E}_c||_{L^2(K)}.$$

The last term on the right-hand side of (4.12) is bounded using the continuity if the bilinear form. Combining all the above bounds and using Lemma 4.1 to bound the nonconforming part, the result follows. □

A posteriori error estimate for the ADG-MS is given below.

THEOREM 4.6. *Let u, U be defined in* (2.1)-(2.2) *and* (3.12)*, respectively and set $\mathcal{I}_h^c U\in H^1(\Omega)$. Set $\mathscr{E}:=\mathscr{E}_c+\mathscr{E}_d$ where $\mathscr{E}_c:=u-\mathcal{I}_h^c U$ and $\mathscr{E}_d:=\mathcal{I}_h^c U-U$. Define $U_{K_H}:=\sum_{j\in\mathcal{M}_{K_H}}U_j(\phi_j+\tilde{\mathcal{T}}\phi_j)+U_{f,K_H}$, where U_j are the nodal values calculated by* (3.11) *for all $\mathcal{K}_H$. Then, $\mathscr{E}$ satisfies the estimate*

$$|||\mathscr{E}||| \lesssim (\sum_{K\in\mathcal{K}}\varrho_K^2)^{1/2}+(\sum_{K\in\mathcal{K}}\zeta_K^2)^{1/2}+(\sum_{K_H\in\tilde{\mathcal{K}}_H}\rho^2_{\omega^L_{K_H}})^{1/2}, \qquad (4.16)$$

where

$$\rho^2_{\omega^L_{K_H}}=\sum_{e\in\Gamma^B(\omega^L_{K_H})}\left(\frac{H^2_{K_H^O}}{h_{K^O}A_0|_{K_H^O}}\right)\left(||n\cdot\{A\nabla U_i\}_w||_{L^2(e)}+\frac{\sigma_e\gamma_e}{h_e}||[U_i]||_{L^2(e)}\right)^2, \qquad (4.17)$$

measures the effect of the truncated patches, K^O, K_H^O are from outside of $\omega^L_{K_H}$, and

$$\begin{aligned}\varrho_K&=\frac{h_K}{\sqrt{A_0}}||(1-\Pi)(f+\nabla\cdot A\nabla U)||_{L^2(K)}, \qquad (4.18)\\ &\quad+\sqrt{\frac{h_K}{A_0}}\Big(||(1-w_{K(e)})n\cdot[A\nabla U]||_{L^2(\partial K)}+||\frac{\sigma_e\gamma_e}{h_e}[U]||_{L^2(\partial K)}\Big),\\ \zeta_K^2&=||\sqrt{A}\nabla(U-\mathcal{I}_h^c U)||^2_{L^2(K)}+||\sqrt{\frac{\sigma_e\gamma_e}{h_e}}[U]||^2_{L^2(\partial K)}. \qquad (4.19)\end{aligned}$$

messuring the refinement level of the fine scale.

REMARK 4.7. *One adaptive strategy is to refine, with a standard a posteriori error bound (e.g. using Theorem 4.3), the coarse mesh as much one can afford, and then further improve the using Theorem 4.6. Note that fine scale problems do not have to be solved everywhere.*

REMARK 4.8. *For the estimator, $\rho_{\omega^L_{K_H}}$, to make sence we have to assume that $H^2_{K_H} \lesssim h_K$. This is not unreasonable since, otherwise each fine scale problem would be more expensive to solve than the coarse scale problem.*

Proof. Using the same idea as in Theorem 4.3. We first, note that

$$|||\mathscr{E}_c|||^2 = a(\mathscr{E}_c, \mathscr{E}_c) = a(\mathscr{E}, \mathscr{E}_c) - a(\mathscr{E}_d, \mathscr{E}_c). \tag{4.20}$$

Then, using (2.9) and the fine scale equations (3.9)–(3.10), we have

$$\begin{aligned} a(\mathscr{E}, \mathscr{E}_c) &= \ell(\mathscr{E}_c) - a(U, \mathscr{E}_c), && (4.21)\\ &= \ell(\mathscr{E}_c - v_H) - a(U, \mathscr{E}_c - v_H), && (4.22)\\ &= \ell(\mathscr{E}_c - v_H - v_f) - a(U, \mathscr{E}_c - v_H - v_f) + \ell(v_f) - a(U, v_f), && (4.23) \end{aligned}$$

for any $v_H \in \mathcal{V}_H$ and $v_f \in \mathcal{V}_f$. Note that,

$$\begin{aligned} \ell(v_f) - a(U, v_f) &= \sum_{K_H \in \tilde{\mathcal{K}}_H} \ell(\chi_{K_H} v_f) - a(U_{K_H}, v_f) && (4.24)\\ &= \sum_{K_H \in \tilde{\mathcal{K}}_H} \sum_{e \in \Gamma^B(\omega^L_{K_H})} \Big((n \cdot \{A\nabla U_i\}_w, [\xi^L_{K_H} v_f])_{L^2(e)} && (4.25)\\ &\quad + (n \cdot \{A\nabla \xi^L_{K_H} v_f\}_w, [U_i])_{L^2(e)} - \frac{\sigma_e \gamma_e}{h_e} ([U_i], [\xi^L_{K_H} v_f])_{L^2(e)} \Big), \end{aligned}$$

where $\xi^L_{K_H} = 0$ on $\omega^L_{K_H}$ and $\xi^L_{K_H} = 1$ otherwise, i.e. $v_f = \xi^L_{K_H} v_f + (1 - \xi^L_{K_H}) v_f$ where $(1 - \xi^L_{K_H}) v_f \in \mathcal{V}_f(\omega^L_{K_H})$. Then, applying (4.25), we deduce

$$\begin{aligned} a(\mathscr{E}, \mathscr{E}_c) &= \Big(\ell(\mathscr{E}_c - v_H - v_f) - a(U, \mathscr{E}_c - v_H - v_f) \Big) && (4.26)\\ &\quad + \sum_{K_H \in \tilde{\mathcal{K}}_H} \sum_{e \in \Gamma^B(\omega^L_{K_H})} \Big((n \cdot \{A\nabla U_i\}_w, [\xi^L_{K_H} v_f])_{L^2(e)} \\ &\quad + (n \cdot \{A\nabla \xi^L_{K_H} v_f\}_w, [U_i])_{L^2(e)} - \frac{\sigma_e \gamma_e}{h_e} ([U_i], [\xi^L_{K_H} v_f])_{L^2(e)} \Big) \\ &=: I + II. \end{aligned}$$

Term I can be estimated as in the proof of Theorem 4.3, upon selecting $v_H := \pi_H \mathscr{E}_c$ and $v_f = \pi_f(\mathscr{E}_c - \pi_H \mathscr{E}_c) = \pi_f \mathscr{E}_c$, where π_H and π_f are the element-wise constant L^2-orthogonal projections onto the coarse space $\mathcal{V}_H$ on the fine space $\mathcal{V}_f$, respectively. We note that, by construction, $\pi_f \pi_H v = 0$, for all $v \in \mathcal{V}_h$.

Since v_f is chosen to be piecewise constant the second term in II is equal to zero. For each $K \in \mathcal{K}$, and for each $e \in \Gamma^B(\omega^L_{K_H}) \backslash \Gamma^B$, we have

$$\begin{aligned} &\Big| (n \cdot \{A\nabla U_i\}_w, [\xi^L_{K_H} v_f])_{L^2(e)} - \frac{\sigma_e \gamma_e}{h_e} ([U_i], [\xi^L_{K_H} v_f])_{L^2(e)} \Big| \\ &\quad \lesssim \Big(||n \cdot \{A\nabla U_i\}_w||_{L^2(e)} + \frac{\sigma_e \gamma_e}{h_e} |||[U_i]|||_{L^2(e)} \Big) |||[\xi^L_{K_H} v_f]|||_{L^2(e)}, \end{aligned} \tag{4.27}$$

using (4.28) and the Cauchy-Schwarz inequality, for $e \in \Gamma^B$, the first term in (4.27) disappears. Note that, $|||[\xi^L_{K_H} v_f]|||_{L^2(e)}$ is either $|||[v_f^+]|||_{L^2(e)}$ or $|||[v_f^-]|||_{L^2(e)}$ depending

on $\xi^L_{K_H}$. To bound the term involving v_f, for simplicity let v_f be either v_f^+ or v_f^-, we note that:

$$\begin{aligned}||v_f||_{L^2(e)} &\lesssim \frac{1}{\sqrt{h_K}}\|v_f\|_{L^2(K)} \lesssim \frac{1}{\sqrt{h_K}}\|v_f\|_{L^2(K_H)} \\ &\lesssim \frac{1}{\sqrt{h_K}}||\mathscr{E}_c - \pi_H\mathscr{E}_c||_{L^2(K_H)} \quad \lesssim \frac{H_{K_H}}{\sqrt{h_K}}||\nabla\mathscr{E}_c||_{L^2(K_H)} \\ &\lesssim \frac{H_{K_H}}{\sqrt{h_K A_0}}||\sqrt{A}\nabla\mathscr{E}_c||_{L^2(K)}, \end{aligned} \tag{4.28}$$

using a trace inequality, and the L^2-stability of π_f, viz., $||\pi_f v||_{L^2(K_H)} \leq ||v||_{L^2(K_H)}$.

Combining the above and summing over all patches, using the discrete version of the Cauchy-Schwarz inequality, the proof is concluded. ∎

5. Implementation and Adaptivity. The system of equations arising from the discretization of the modified coarse multiscale problem (3.11) is given by

$$KU = b - d, \tag{5.1}$$

where $K_{i,j} = a(\phi_j + \tilde{\mathcal{T}}\phi_j, \phi_i)$, $b_i = \ell(\phi_i)$, and $d_i = a(U_f, \phi_i)$. To assemble the right and left hand sides of (5.1), $\tilde{\mathcal{T}}\phi_i$ and $U_{f,i}$ need to be computed for all $i \in \mathcal{N}$. This can be done in parallel since no commutation is needed between the different fine scale problems. For each fine scale problem it is also possible to assemble $K_{i,j} = a(\phi_j + \tilde{\mathcal{T}}\phi_j, \phi_i)$, $b_i = \ell(\phi_i)$, and $d_i = \sum_{j\in\mathcal{N}} a(U_{f,j}, \phi_i)$ for a fixed i and for all j such that $\mu_d(\text{supp}(\phi_j) \cap \bar{\omega}_K) > 0$. The constraints needed on the fine scale test spaces to solve $\tilde{\mathcal{T}}\phi_i$ and $U_{f,i}$ are $\mathcal{V}_f = \{v \in \mathcal{V}^h : \Pi_H v = 0\}$, which are implemented using Lagrange multipliers. The spaces $\mathcal{V}_f$ and $\mathcal{V}_H$ are orthogonal with respect to the L^2-inner product.

Let $\mathcal{V}_H = \text{span}\{\phi_i\}$ and $\mathcal{V}_f = \text{span}\{\varphi_i\}$. Then, the system of equations to be solved on the fine scale is given by

$$\begin{pmatrix} K & P^T \\ P & 0 \end{pmatrix} \xi = \begin{pmatrix} b \\ 0 \end{pmatrix}, \tag{5.2}$$

where

$$P = \begin{pmatrix} (\phi_1,\varphi_1) & (\phi_1,\varphi_2) & \dots & (\phi_1,\varphi_N) \\ (\phi_2,\varphi_1) & (\phi_2,\varphi_2) & \dots & (\phi_2,\varphi_N) \\ \vdots & \vdots & \ddots & \vdots \\ (\phi_M,\varphi_1) & (\phi_M,\varphi_2) & \dots & (\phi_M,\varphi_N) \end{pmatrix}, \tag{5.3}$$

with $K_{k,l} = a_i(\varphi_k, \varphi_l)$ and b either $b_k = l_i(\varphi_k)$ for (3.10) or $b_k = -a_i(\phi_i, \varphi_k)$ for (3.9).

Using the a posteriori error estimate above it is possible to design an adaptive algorithm that automatically tunes the fine mesh size and the size of the patches. In the numerical experiments below, we have implemented Algorithm 1, which extends the patches in all directions and uses a uniform mesh refinement of the fine scale on each coarse element. A more elaborate algorithm which only extends in the direction where the error is large and uses adaptive mesh refinement would be a possible extension, since the a posteriori indicators above contain local contributions of each individual patch-boundary face and of each fine scale element residual.

Algorithm 1 Adaptive Discontinuous Galerkin Multiscale Method

Initialize the coarse mesh, $\mathcal{K}_H$ with mesh function H, and a fine mesh, $\mathcal{K}_h$ with meshfunction h, by using to uniform refinements of $\mathcal{K}_H$ i.e., h = H/4.
For all $\mathcal{K}_H$ let the size of the patches be $\omega^3_{K_H}$.
Set the mesh refinment level to X%.
while $(\sum_{K\in\mathcal{K}} \varrho^2_{h,K})^{1/2} + (\sum_{K\in\mathcal{K}} \zeta^2_{h,K})^{1/2} + (\sum_{K_H\in\mathcal{K}_H} \rho^2_{\omega^L_{K_H}})^{1/2} > TOL$ **do**
    for $K \in \tilde{\mathcal{K}}_H$ **do**
        Solve the fine scale problems (3.1) and (3.10).
        Compute the matrix and vector entries on the coarse scale (5.1).
    end for
    Solve the modified coarse scale problem (3.11).
    Mark the indicator with X% largest error in $\{\varrho^2_{h,K} + \zeta^2_{h,K}, \rho^2_{L,\omega_i}\}$.
    for $K_H \in K_H$ **do**
        if ρ^2_{L,ω_i} is marked **then**
            $\omega^L_{K_H} := \omega^{L+1}_{K_H}$
        end if
        if $\rho^2_{h,K} + \zeta^2_{h,K}$ is marked **then**
            $h|_{K_H} := h|_{K_H}/2$
        end if
    end for
end while

6. Numerical examples. We present some numerical experiments where the converge of the method as well as the performance of the adaptive algorithm is investigated.

6.1. Convergence. We consider the model problem (2.1)–(2.2) on the L-shaped domain constructed by removing the lower right quadrant in the unit square, with forcing function $f = 1$. We consider a coarse quadrilateral mesh of size $H = 2^{-4}$. Furthermore each coarse element $K \in \mathcal{K}_H$ is further subdivided using two uniform refinements to construct the fine mesh. The error is measured in the relative energy norm, (2.12), where u_h is the DG solution on the fine mesh i.e., there is only a truncation error (due to the fine scale patch size) between the multiscale solution and the DG solution. The permeabilities *One* and *SPE*[1], illustrated in Figure 6.1, are used. In *One*, we have $A = 1$, and in *SPE* the data is taken from the tenth SPE comparative solution project and is projected into the fine mesh. Exponential decay is observed with respect to the number of layers for the different permeabilities *One* and *SPE*, until the patches covers the whole domain when $L = 8$; this is illustrated in Figure 6.2. As expected, when $L = 8$, only round off error between the multiscale solution and the reference solution is observed. Note that we have convergence to u_h sine the right hand side correction fine scale correction is included.

6.2. Adaptivity for a problem with analytic solution. Let us consider the model problem (2.1)–(2.2) on a unit square, using the permeability, $A = 1$, and the forcing function, $f = 4a^2(1 - ar^2)e^{-ar^2}$. Using $a = 400$, the analytic solution can be approximated sufficiently well by $u = ae^{-ar^2}$, which represent a Gaussian pulse in the middle of the domain. Consider a coarse quadrilateral mesh of size $H = 2^{-4}$,

[1]Data is taken from the tenth SPE comparative solution project http://www.spe.org/web/csp/

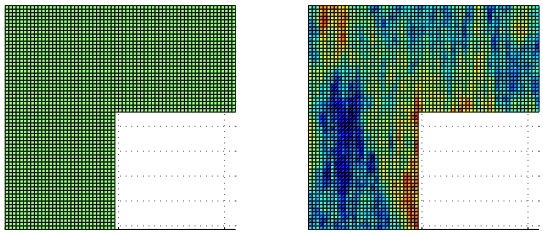

FIGURE 6.1. *Permeability structure of* One *and* SPE *in log scale on a L-shaped domain.*

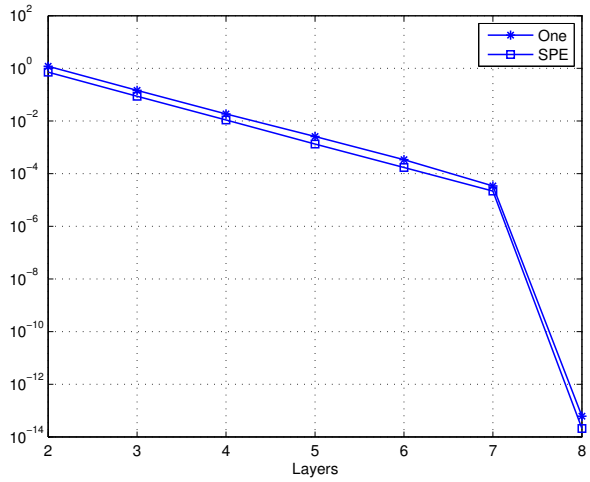

FIGURE 6.2. *Convergence in relative energy norm* (2.12)*, on a L-shaped domain when the number of layers are increased using the different permeabilities* One *and* SPE*.*

and a fine mesh of size $h = 2^{-6}$. The adaptive algorithm (Algorithm 1) with 10% refinement level is used. The starting values in the adaptive algorithm are, that each patch consist of 3 layers and the fine scale mesh are uniformly refined two times. Figure 6.3 shows the how the error and error indicators decrease in each iteration of the adaptive algorithm and Figure 6.4 show were the adaptive algorithm put the computational effort, which is in the position of the pulse.

6.3. Adaptivity on an L-shaped domain. Consider the model problem and the same data as in Section 6.1. An adaptive algorithm is used where multiscale solution is compared to a reference solution computed with the standard DG solution on a uniform quadrilteral mesh with mesh size $h = 2^{-9}$, see Figure 6.3. Let the coarse mesh consist of a uniform quadrilteral mesh of size $H = 2^{-4}$. The starting values in the adaptive algorithm (Algorithm 1) are that each patch consist of 3 layers ($L = 3$) and the fine scale mesh are two uniform refinments of the coarse mesh. In each iteration a refinment level of 30% is used. Figure 6.3 shows how the error decreases after each iteration in the adaptive algorithm. Also, the adaptive algorithm chooses to increase the patches in the beginning since the error from the truncation is initially larger than the discretization error and after a few iterations it is starting

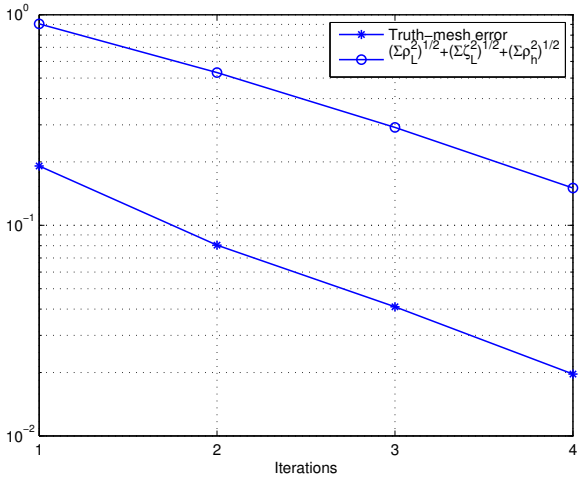

FIGURE 6.3. *Convergence in relative energy norm 2.12, using a adaptive algorithm on the unite square with Gaussion puls in the middle.*

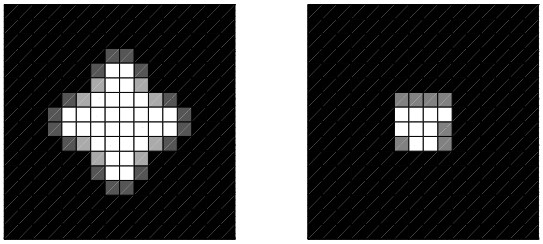

FIGURE 6.4. *The level of refinement and size of the patches illustrated in the left resp. right plots, using a adaptive algorithm on a unite square with Gaussion puls in the middle. White is where most refinements resp. bigger size are used and black is where least refinements resp. smallest patches are used.*

to refine the fine scale mesh more and more. When the patch sizes are increased the error, due to truncation, decays exponentially independent of the regularity of the solution as shown theoretically in [17]. This is not true for the discretization error. This motivates the use of an adaptive algorithm which tune the error between the truncation and discretization. Figure 6.7 shows where the adaptive algorithm put most computational effort.

6.4. Adaptivity for flow in porous media. We consider the problem (2.1)–(2.2) on the unit square $\Omega = [0,1]^2$, with forcing function $f = -1$ in the lower left corner $\{0 \leq x, y \leq 1/128\}$, $f = 1$ in the upper right corner $\{127/128 \leq x, y \leq 1\}$, and $f = 0$ otherwise. The following permeabilities *SPE11* and *SPE21* are used and projected into a mesh with 64×64 elements, see Figure 6.8. The computational domain Ω is split into 32×32 coarse square elements $K_H \in \mathcal{K}_H$. The error is measured in the relative energy norm, with the reference solution u_h being the DG solution computed on a 512×512-element mesh. The adaptive algorithm (Algorithm 1) with

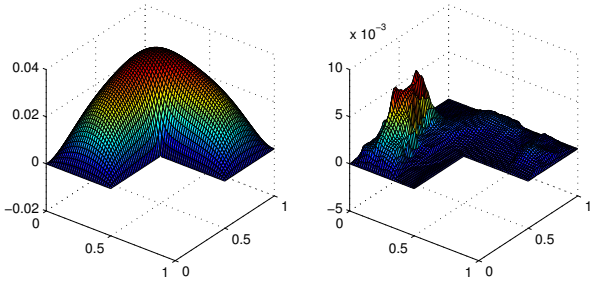

FIGURE 6.5. *Reference solution for the different permeabilities computed on a mesh with size* $h = 2^{-9}$ *and projected to a mesh with size* $h = 2^{-6}$.

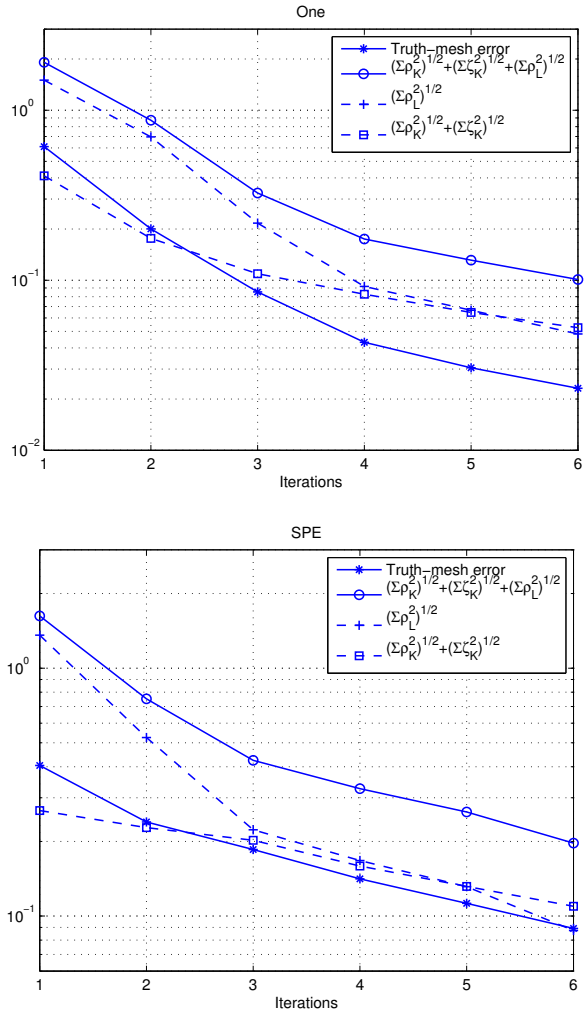

FIGURE 6.6. *The relative error in energy norm for the multiscale solution using the adaptive algorithm and where,* ρ_L *is the truncation error indicator,* ϱ_K *and* ζ_K *are the discretization error indicators.*

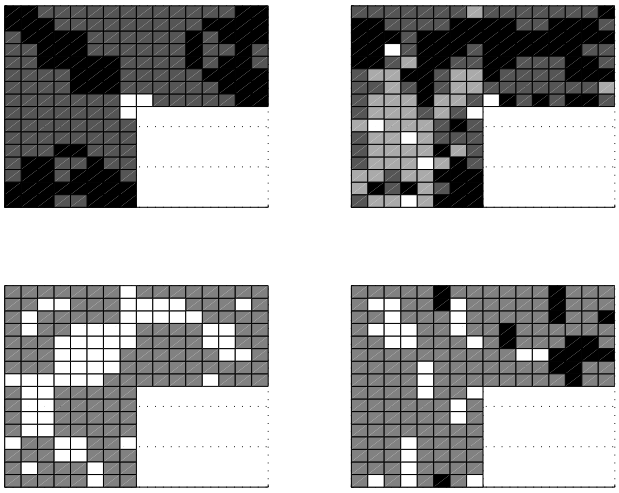

FIGURE 6.7. *The level of refinement and size of the patches illustrated in the upper resp. lower plots for the different permeability One (left) and SPE (right). White is where most refinements resp. larger patch are used and black is where least refinements resp. smallest patches are used.*

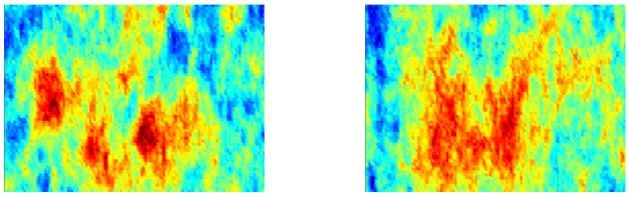

(a) SPE11, $\alpha_{max}/\alpha_{min} = 6.1765 \cdot 10^5$ (b) SPE21, $\alpha_{max}/\alpha_{min} = 5.0193 \cdot 10^5$

FIGURE 6.8. *Permeabilities projection in log scale.*

refinment level 30% are used. In Iteration 1 the multiscale problem is solved using two refinement on each coarse element and each fine scale problem is solved with $L = 3$, and so on. Even though complicated permeabilities with $\alpha_{max}/\alpha_{min} \sim 10^5$ are used, the proposed adaptive algorithm is able to reduce relative error considerably; this is shown in Figure 6.9.

7. Concluding remarks. An adaptive multiscale method based on discontinuous Galerkin discretization has been proposed and assessed in practice. There are several different advantages for using the proposed multiscale method. The possibility to allow a global underling reference grid (using the DG framework including hanging nodes) is crucial. This does not only account for cancellation of the error between different fine scale problems in the a posteriori error bound, it also fits the method into the convergence framework presented in [17]. It admits a local conservation of the state variable, which is crucial in many applications e.g. prous media flow. The mul-

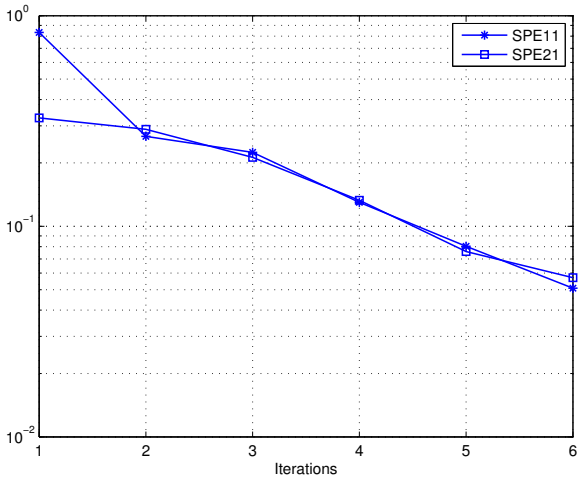

FIGURE 6.9. *Relative in error broken energy norm against the number of iterations using the adaptive algorithm for flow in porous media.*

tiscale method and the adaptive algorithm admit naturally parallel implementation, which results in further savings in computational time.

An adaptive algorithm for which the coarse scale, the fine scale, and the size of the different patches are taken into account, based on an energy norm a posteriori bound is proposed. Using the proposed multiscale method together with the adaptive algorithm lead to substantial computational savings and perform very well when applied to challenging benchmark problems.

REFERENCES

[1] J. Aarnes and B.-O. Heimsund, *Multiscale discontinuous Galerkin methods for elliptic problems with multiple scales*, Lecture Notes in Computational Science and Engineering, vol. 44, Springer Berlin Heidelberg, 2005.

[2] A. Abdulle, *Discontinuous Galerkin finite element heterogeneous multiscale method for elliptic problems with multiple scales*, To appear http://dx.doi.org/10.1090/S0025-5718-2011-02527-5, 2011.

[3] R. A. Adams, *Sobolev spaces*, Academic Press, New York, 1975.

[4] M. Ainsworth, *Robust a posteriori error estimation for nonconforming finite element approximation*, SIAM Journal on Numerical Analysis **42** (2005), no. 6, pp. 2320–2341.

[5] D. N. Arnold, *An interior penalty finite element method with discontinuous elements*, SIAM J. Numer. Anal. **19** (1982), no. 4, 742–760.

[6] D. N. Arnold, F. Brezzi, B. Cockburn, and L. Marini, *Unified analysis of discontinuous Galerkin methods for elliptic problems*, SIAM J. Numer. Anal. **39** (2001), no. 5, 1749–1779.

[7] I. Babuška, G. Caloz, and J. E. Osborn, *Special finite element methods for a class of second order elliptic problems with rough coefficients*, SIAM J. Numer. Anal. **31** (1994), no. 4, 945–981.

[8] I. Babuška and J. E. Osborn, *Generalized finite element methods: their performance and their relation to mixed methods*, SIAM J. Numer. Anal. **20** (1983), no. 3, 510–536.

[9] G. A. Baker, *Finite element methods for elliptic equations using nonconforming elements*, Math. Comp. **31** (1977), no. 137, 45–59.

[10] E. Burman and P. Zunino, *A domain decomposition method based on weighted interior penalties for advection-diffusion-reaction problems*, SIAM J. Numer. Anal. **44** (2006), no. 4, 1612–1638 (electronic). MR 2257119 (2007m:65123)

[11] Z. Cai, X. Ye, and S. Zhang, *Discontinuous galerkin finite element methods for interface prob-*

lems: A priori and a posteriori error estimations, SIAM Journal on Numerical Analysis **49** (2011), no. 5, 1761–1787.

[12] J. Chu, Y. Efendiev, V. Ginting, and T. Y. Hou, *Flow based oversampling technique for multiscale finite element methods*, Advances in Water Resources **31** (2008), no. 4, 599–608.

[13] B. Cockburn, G. E. Karniadakis, and C-W. Shu (eds.), *Discontinuous Galerkin methods*, Lecture Notes in Computational Science and Engineering, vol. 11, Springer-Verlag, Berlin, 2000, Theory, computation and applications, Papers from the 1st International Symposium held in Newport, RI, May 24–26, 1999.

[14] D. A. Di Pietro and A. Ern, *Mathematical aspects of discontinuous galerkin methods*, Mathématiques et Applications, vol. 69, Springer, 2012.

[15] W. E, *Principles of multiscale modeling*, Mathematical Modeling and Methods, Cambridge University Press, 2011.

[16] Y. Efendiev and T. Y. Hou, *Multiscale finite element methods*, Surveys and Tutorials in the Applied Mathematical Sciences, vol. 4, Springer, New York, 2009, Theory and applications.

[17] D. Elfverson, E. H. Georgoulis, A. Målqvist, and D. Peterseim, *Convergence of a discontinuous Galerkin multiscale method*, Submitted for publication, available as preprint arXiv:1211.5524 (2012).

[18] A. Ern and A.F. Stephansen, *A posteriori energy-norm error estimates for advection-diffusion equations approximated by weighted interior penalty methods*, J. Comput. Math. **26** (2008), no. 4, 488–510.

[19] A. Ern, A.F. Stephansen, and P. Zunino, *A discontinuous Galerkin method with weighted averages for advection-diffusion equations with locally small and anisotropic diffusivity*, IMA Journal of Numerical Analysis **29** (2009), no. 2, 235–256.

[20] J. S. Hesthaven and T. Warburton, *Nodal discontinuous Galerkin methods*, Texts in Applied Mathematics, vol. 54, Springer, New York, 2008, Algorithms, analysis, and applications.

[21] T. Y. Hou, T. Y. Hou, and X.-H. Wu, *A multiscale finite element method for elliptic problems in composite materials and porous media*, Journal of Computational Physics **134** (1997), 169–189.

[22] T. Hughes, *Multiscale phenomena: Green's functions, the Dirichlet-to-Neumann formulation, subgrid scale models, bubbles and the origins of stabilized methods*, Computer Methods in Applied Mechanics and Engineering **127** (1995), no. 1-4, 387–401.

[23] T. Hughes, G. Feijóo, L. Mazzei, and J.-B. Quincy, *The variational multiscale method–a paradigm for computational mechanics*, Computer Methods in Applied Mechanics and Engineering **166** (1998), no. 1-2, 3 – 24.

[24] C. Johnson and J. Pitkäranta, *An analysis of the discontinuous Galerkin method for a scalar hyperbolic equation*, Math. Comp. **46** (1986), no. 173, 1–26.

[25] O. Karakashian and F. Pascal, *A posteriori error estimates for a discontinuous Galerkin approximation of second-order elliptic problems*, SIAM J. Numer. Anal. **41** (2003), 2374–2399.

[26] O. Karakashian and F. Pascal, *Adaptice discontinuous Galerkin approximation of secound-order elliptic problems*, In Proceedings of the European Congress on Computational Methods in Applied Sciences and Engineering ECCOMAS 2004. P. Neittaanmäki et al. eds. Jyväsklä, 24-28 July 2004.

[27] M. G. Larson and A. Målqvist, *Adaptive variational multiscale methods based on a posteriori error estimation: Energy norm estimates for elliptic problems*, Computer Methods in Applied Mechanics and Engineering **196** (2007), no. 21-24, 2313–2324.

[28] P. Lesaint and P.-A. Raviart, *On a finite element method for solving the neutron transport equation*, Mathematical aspects of finite elements in partial differential equations (Proc. Sympos., Math. Res. Center, Univ. Wisconsin, Madison, Wis., 1974), Math. Res. Center, Univ. of Wisconsin-Madison, Academic Press, New York, 1974, pp. 89–123. Publication No. 33.

[29] A. Malqvist, *Multiscale methods for elliptic problems*, Multiscale Modeling & Simulation **9** (2011), no. 3, 1064–1086.

[30] A. Målqvist and D. Peterseim, *Localization of elliptic multiscale problems*, Submitted for publication in Math. Comp., in revision, available as preprint arXiv:1110.0692 (2011).

[31] M. Petzoldt, *A posteriori error estimators for elliptic equations with discontinuous coefficients*, Advances in Computational Mathematics **16** (2002), 47–75.

[32] W. H. Reed and T. R. Hill, *Triangular mesh methods for the neutron transport equation.*, Tech. report, Los Alamos Scientific Laboratory, 1973.

[33] B. Rivière, *Discontinuous Galerkin methods for solving elliptic and parabolic equations*, Frontiers in Applied Mathematics, vol. 35, Society for Industrial and Applied Mathematics (SIAM), Philadelphia, PA, 2008, Theory and implementation.

[34] W. Wang, *Multiscale discontinuous Galerkin methods and applications*, ProQuest LLC, Ann

Arbor, MI, 2008, Thesis (Ph.D.)–Brown University.

[35] W. Wang, J. Guzmán, and C.-W. Shu, *The multiscale discontinuous Galerkin method for solving a class of second order elliptic problems with rough coefficients*, Int. J. Numer. Anal. Model. **8** (2011), no. 1, 28–47.

[36] L. Yuan and C.-W. Shu, *Discontinuous Galerkin method based on non-polynomial approximation spaces*, J. Comput. Phys. **218** (2006), no. 1, 295–323.

[37] L. Yuan and C.-W. Shu, *Discontinuous Galerkin method for a class of elliptic multi-scale problems*, Internat. J. Numer. Methods Fluids **56** (2008), no. 8, 1017–1032.